Invited Articles

Flows, self-organization, and transport in living cells

Michael J. Shelley
Center for Computational Biology, Flatiron Institute, New York 10010, USA
and Applied Math Lab, Courant Institute, New York University, New York 10012, USA

(Received 2 August 2024; accepted 5 November 2024; published 11 December 2024)

This paper briefly reprises, with added commentary, a talk I gave on transport and flows within living cells at an APS-DFD meeting. Directed transport is especially important in large cells, such as eggs where developmental factors need to be properly localized, and early embryos whose organelles and genetic material must be properly positioned before cell division. I discuss two cases—a nematode single-cell embryo and a fruit fly egg cell—where advances in mathematical modeling and large-scale simulation of fluid-structure interactions have helped us understand fundamental mechanisms of force transduction and self-organization within the cell.

DOI: 10.1103/PhysRevFluids.9.120501

I. INTRODUCTION

To start, it will be helpful to cover some basic biology. At least on Earth, the basic unit of life is the cell. The movement of components both in and out of cells is highly controlled and so each cell is, to greater or lesser degrees, its own metropolis. But quite unlike our own cities, the cell's neighborhoods and transportation networks are not fixed to some solid ground but are instead floating, deformable, and often transitory. Despite their small sizes, typically $2-30\,\mu$m [1] but sometimes stretching up to hundreds of microns or more, cells have a daunting complexity of components and interactions made possible by their now billions of years of evolution.

Cells have many active transport processes, some of which involve fluid flows facilitated by the cell's so-called cytoskeleton. Rather than being a structure, as the name suggests, the cytoskeleton is actually a set of components – biopolymers such as actin and microtubules, molecular cross-linkers and motors, and other proteins—that are used within the cell to support loads, transmit forces, and carry payloads. Microtubules are particularly central to this discussion, being relatively stiff polar polymers whose persistence length is well beyond the cell size, and which grow at their so-called plus ends; see Gittes *et al.* [2]. The cytoskeleton can self-organize to assemble functional structures within the cell, such as the spindle complexes that orchestrate chromosomal division, polymer meshworks that alter the mechanics of the cell, or polymer beds lining cells upon which motor proteins can act to produce surface forces. These structures are immersed and move against the cell's fluidic interior, the cytoplasm, which is itself an aqueous slurry packed with a variety of objects like vesicles, polymers, and protein condensates [3]. This is the flowing medium of the cell, which is commonly treated as a highly viscous, Newtonian fluid. This assumption is (possibly) reasonable so long as the motions being studied are slow enough not to excite other mechanics, such as elasticity. While cytoplasmic flows can be part of the cell's transport machinery, they are also, at the least, an inevitable consequence of the cytoskeletal structures moving through the cytoplasm; see Needleman and Shelley [4] for a recent review of some of these issues.

In my DFD talk, I focused on egg cells and early embryos, as I do here. Egg cells, called oocytes by biologists, are special. When fertilized, and so becoming an embryo, the cell must contain all the components needed for producing a multicellular organism. Hence, they tend to be large, having sizes from $\sim 50\,\mu$m up to several centimeters. Their larger size has made them attractive for studying,

via light microscopy in model organisms, the very first cell divisions and the early development of an organism. As I hope the reader will appreciate, these studies illustrate the explanatory (or at least conjectural) power gained by marrying modern tools of coarse-grain modeling and large-scale simulation to sophisticated, well-designed experiments of cellular-scale biophysics.

II. CYTOPLASMIC FLOWS IN CELLS

A. A partial history

The flow of cytoplasm, often termed cytoplasmic streaming, occurs in a variety of cells and settings. It is not surprising that early observations were made in large cells, not only because of the relative ease of observation but because diffusion becomes ineffective as a transport mechanism and other means of intracellular transport become necessary. Early observations of streaming were made by the Italian priest Bonavetura Corti (1729-1813) [5] in the multicellular green algae *Chara* whose so-called internodal cells can be exceptionally large (reaching centimeters). These flows, further studied and nicely reviewed by Goldstein and van de Meent [6], are generated by myosin molecular motors carrying payloads along a structured polymeric actin backbone attached to the cell boundary. Interestingly, the Englishman Robert Brown (1773-1858), of Brownian motion fame, also observed, at least in my reading, streaming flows within large plant cells [7]. As a last historical example, the German biologist Franz Schulze (1815-1873) observed streaming in the crawling giant ameboid cell *Pelomyxa pelustrus*, with that flow presumably arising from its locomotion; see Pickens [8]. Mogilner and Manhart [9] give a modern review.

B. Flows in two model organisms

Many contemporary observations and studies of cytoplasmic flows have been on the egg cells and embryos of model organisms, particularly the nematode *Caenorhabditis elegans* and the fruit fly *Drosophila melanogaster*, but have also been observed in other organisms such as in mouse oocytes [10]. With fertilization of the *C. elegans* egg, sequential streaming flows develop that first involve interactions of microtubules with the endoplasmic reticulum (see Kimura *et al.* [11]) and then contractions driven by the molecular motor myosin of an actin polymer meshwork lining the cell boundary; see, for example, Hird and White [12] and Mayer *et al.* [13]. These flows organize the contents of the cell and set up the polarity of the cell, yielding an asymmetric first cell division and the eventual body plan of the developed organism. The latter contraction-driven flows also participate in setting up the next stage of embryonic development by helping push the female pronucleus—the egg's contribution to the progeny—from the anterior side of the embryo towards the male pronucleus at the posterior. Gubieda *et al.* [14] provided a recent review.

The dynamics that follows is complex [15,16] [see Figs. 1(a) and 1(b)], involving centrosomal asters which are arrays of thousands of transitory microtubules that emanate from two mobile nucleating sites—centrosomes—that arrived with the sperm to the egg. Asters are capable of supporting loads and transferring forces and these two asters seemingly negotiate a series of maneuvers of the pronuclei, first bringing them together, then positioning them near the center of the cell through a translation and rotation that leaves the asters on the cell's long axis. The now fused pronuclei transition into a mitotic spindle, encapsulating condensed duplicated chromosomes, which stretches asymmetrically towards the posterior of the cell. This sets up the first cell division.

In my APS-DFD talk, I discussed how the structure of the cytoplasmic flows associated with all these motions helped resolve a long-standing question: How exactly are the forces produced that drive this complicated and endlessly repeated dance? Here is a good point to digress and discuss what tools are now available to address such a question.

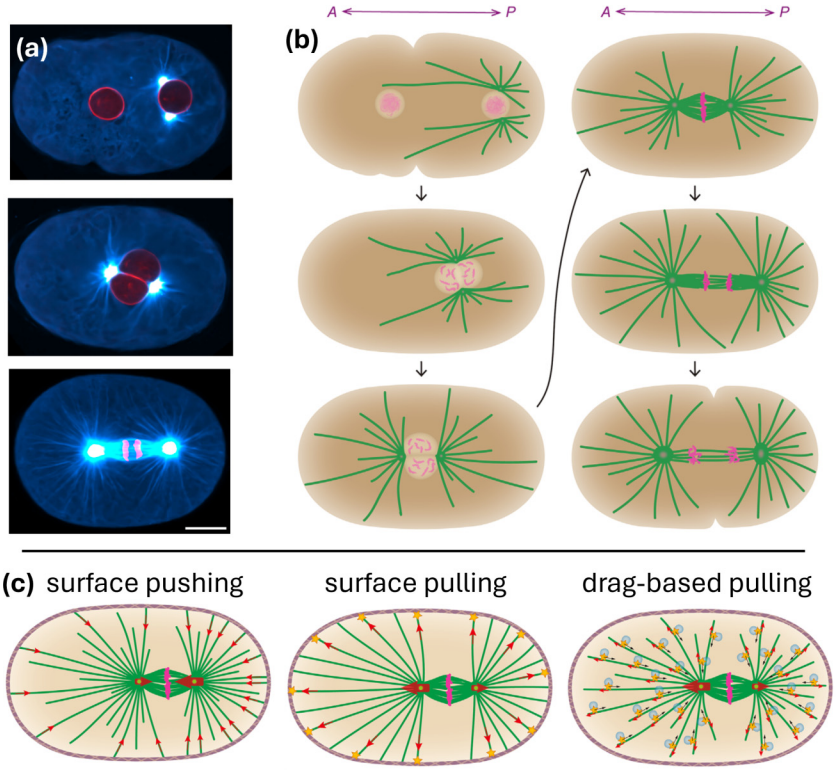

FIG. 1. (a) Using fluorescent labeling of microtubules (blue) and DNA (red), microscopy images of positioning and segregation dynamics of genetic material within a single-cell *C. elegans* embryo. Centrosomes sit within the bright blue foci from which nearly linear microtubules emanate. Scale bar is 10 μm; courtesy of R. Farhadifar (Flatiron CCBScope). (b) A schematic representation, with microtubules in green and DNA in blue, of the succession of stages—pronuclear attraction, migration, centering, spindle formation with chromosome condensation, and spindle elongation with chromosome segregation—of genetic material disposition as the first cell division is approached. (c) Three models of force transduction: cortical pushing wherein microtubules polymerize against the cell boundary (left), surface pulling wherein microtubules are pulled by motor proteins anchored to the cell boundary (center), and drag-based pulling wherein motor proteins carry payloads along microtubules towards the centrosome (right); panels (b) and (c) are adapted from Wu *et al.* [15].

C. Experimental techniques for intracellular phenomena

There have been tremendous advances in measurement and observation of cellular dynamics. Many methods now exist for tagging, and so visualizing via light microscopy, specific proteins with fluorescing proteins. Tagging of the tubelin dimers that compose microtubules allows a coarse-grained view of the evolving microtubule-based structures like spindles and asters, inside of living cells; Fig. 1(a) provides an example. Other microscopy methods exist for measuring nematic and polar order of polymer assemblies, even inside of cells. For finely detailed views of cellular structures, one can turn to electron microscopy and tomography which examine, with great labor, individual cells fixed at particular stages of their evolution [17]. Other methods directly perturb the inner workings of the cell, such as through RNA interference [18], which inhibits expression of specific genes, and so alters the downstream production of the proteins involved in these processes. However, genes usually function as parts of gene networks and it can be difficult to know exactly how, and by how much, the functioning of the cell is changed by such methods.

Other methods more directly address the questions at hand. In particular, our Harvard collaborators developed a precise method of rapidly severing, using a laser, any microtubules that pass through a preselected plane or surface within the cell; see Wu *et al.* [16]. When those microtubules are load bearing, the force balance of the system is broken, at least until the microtubules regenerate, and the consequent reaction of attached structures, like centrosomes, is telling. Through careful and repeated application of this method, our colleagues were able to conclude that centrosomes were being actively pulled upon by force generators located on the periphery of the cell. These force generators were presumably dynein molecular motors, tethered to the cell boundary, that bind to microtubules and walk (while held in place) towards the microtubule minus-end at the centrosome, as schematized in Fig. 1(c) (middle panel; surface pulling). This finding contradicts two other possible models, with one postulating pushing forces arising from growing microtubules pushing against the cell boundary [see, e.g., Ref. [19] and left panel of Fig. 1(c)], and the other postulating pulling forces created by payloads being dragged through the cytoplasm and along microtubules [see Refs. [20,21] and right panel of Fig. 1(c)].

D. Modeling and simulation for intracellular biophysics

While experimental techniques have made large strides, so have the numerical methods available to simulate such complex problems. In work spanning over 20 years, we and others have developed robust and efficient methods of simulation of elastic fiber assemblies [22]; in my own work, starting with Tornberg and Shelley [23] (Nazockdast *et al.* [24] details extensions to microtubules and cells while du Roure *et al.* [25] reviews many applications). Our methods rest upon three legs. One is slender-body theory for the Stokes equations that allows one to both efficiently compute the hydrodynamic flows induced from the motion of long thin filaments—read microtubules—moving through a Newtonian fluid, and to compute how such filaments deform in response to flows and their own internal mechanics. In the latter, microtubules show flexural rigidity and near inextensibility. Another important numerical component are boundary integral formulations of the Stokes equations that allow the highly efficient calculation of the back flows from the cell boundary, and solution of mobility problems for any other rigid but mobile objects in the flow, such as modeled centrosomes [26]. The final element is implicit/explicit time-integration methods that stably handle the high-order spatial terms that arise in modeling filament elasticity. Taken all together, when set in a highly parallel computing environment and using fast multipole methods, this suite of methods allows for the efficient simulation of the geometrically complex dynamics of confined microtubule assemblies. This software suite is called SkellySim [27] and some of its theoretical elements are given more explicitly below in the discussion of flows in egg cells. A recent discussion and overview of current numerical and theoretical approaches to cell mechanics can be found in Stein and Shelley [28].

In earlier work, we applied these numerical methods to simulate versions of each of the three force-transduction models discussed above for dynamics of the pronuclear complex during the early positioning stage [26]; in yet earlier work, we used an immersed boundary method to simulate a simplified version of the drag-based pulling model [21]. The end result was that each model could produce, with seemingly reasonable choices of coefficients, proper positioning within an appropriate time. While it was disheartening that simulations didn't pick a definitive model, we also found that the cytoplasmic flows induced by these models could differ. Unsurprisingly, the surface-pulling and -pushing models showed similar internal flows (so long as the pushing model's microtubules didn't buckle) as in both flows are produced by the dragging of microtubules through the cytoplasm. The drag-based pulling model, however, applies forces along immersed microtubules, producing active flows directly within the aster.

E. Integrating experiment and simulation

Given the lack of good experimental data, in Wu *et al.* [16], we examined the nature of cytoplasmic flows in real embryos. In addition to the laser-cutting techniques, our Harvard colleagues also

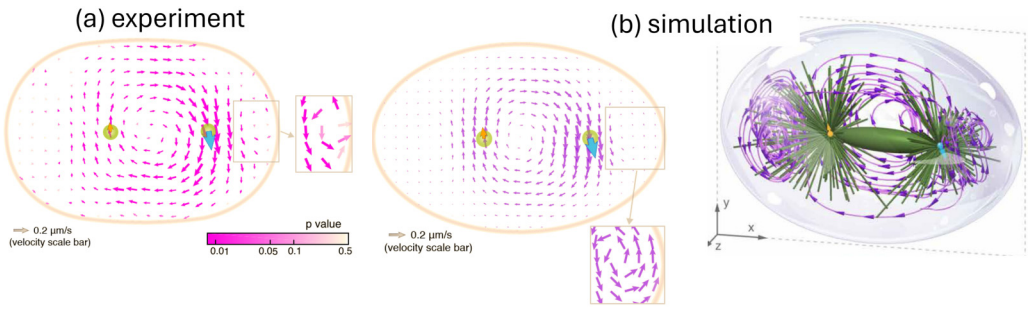

FIG. 2. (a) Average fluid velocity field measured during the elongation and segregation stage when the spindle complex has a brief burst of oscillation. (b) A simulation of the spindle complex at that stage, using SkellySim [27], where microtubules (not shown) emanating from centrosomes are pulled upon by cell surface force generators. Left panel: The velocity field taken from the simulation. Right panel: A volumetric view of the simulation showing the modelled spindle complex (green), centrosomes (gold), and microtubules (green), as well as flow streamlines (purple). Details from the velocity fields of both experiment and simulation show secondary vortices generated by the motion. These are also apparent in the three-dimensional rendering of the simulation. Adapted from Wu *et al.* [16].

developed a particle-imaging velocimetry technique based on the motion of fluorescing nanodiamonds within the developing embryo. These fluorescing particles found their way into embryos by being microinjected into the gonads of parent worms. From the nanodiamond motions, averaged velocity fields at various stages were found by averaging over many nematode embryos; see Fig. 2(a). Using our simulation methods, we instantiated the two pulling models (surface pushing having been ruled out) at stages matching the experiments. In all cases, we found substantial discordance of the experimental results with the drag-based pulling model. Likewise, our simulations of surface pulling showed substantial concordance with the experimental results, down to the existence and placement of secondary vortical structures; see Fig. 2(b). This gave strong support for the dominant role of surface pulling as guiding all stages of nuclear positioning and chromosome segregation prior to cell division.

In summary, while fluid dynamics doesn't play the central organizing role here—motor forces apparently dominate fluid dynamical ones—cytoplasmic flows served as an important signature as to how and where active forces were being produced. Other work has since sprung from this. That surface pulling is the dominant force on centrosomes, iimplying that microtubules bound to surfaces should be under extensile load, and thus not so susceptible to bending. This conception has been moved into a coarse-grain version of centrosomal arrays and populations of surface-bound motors as continua. This model can predict observed frequencies of centrosome oscillations and the force-displacement relation for stably placed asters [16,29]. Current work has graduated such continuum models to study the effect of cell shape on internal dynamics and how centrosomes' competition for surface force generators can drive dynamics during the run-up to cell division.

F. Transport flows in egg cells

While fluid dynamics was not a central organizing determinant of the late stage dynamics in the single-cell *C. elegans* embryo, this is not so for the fruit fly (*D. melanogaster*) egg cell [30]. The fruit fly egg, or oocyte, is grown in a specialized female organ called the egg chamber wherein 15 other cells—nurse cells—collaborate, and die, to give their contents to develop one very large egg cell [31]. In *D. melanogaster*, oocytes grow 50-fold in scale from a standard $\sim$10 μm cell size to a hefty $\sim$500 μm. Biologists have long studied fruit fly oogenesis and have divided the progression of development into a number of discrete stages. In stage 9, are observed small-scale, intermittent

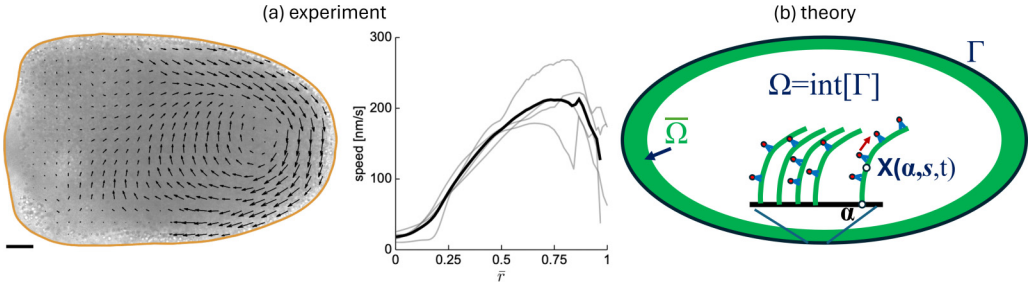

FIG. 3. (a) Experimentally measured fluid velocities within stage 10 in a fruit fly oocyte, using endogenous particles for particle imaging velocimetry. Left panel: The velocity vector field reconstruction in a slide through the ooctye. Middle panel: Measured speeds within the vortex, measured from vortex center to the posterior (right-hand) side of the cell; adapted from Dutta *et al.* [40]. (b) A schematic of a mathematical model wherein a microtubule bed is clamped to the side of the cell. Molecular motors carry payloads up the microtubules, thereby exerting equal and opposite forces on fluid and microtubule. Here Ω is the cell interior with boundary Γ, and $\tilde{\Omega}$ is the subset containing the microtubule bed. The microtubule bed is represented as $\mathbf{X}(\boldsymbol{\alpha}, s, t)$ where $\boldsymbol{\alpha}$ is the boundary coordinate where the microtubule is clamped and s is the arclength of the (inextensible) microtubule, measured from the base [41].

cytoplasmic flows termed seething, while in stage 10, when the oocyte is $\sim$100 μm in scale, there emerge cell-scale flows, sometimes appearing as a vortex [30,32–35] as seen in Fig. 3(a).

There are a number of questions here. One is what problems the egg cell might be addressing through such flows. Its answer might be the maintenance of timely and targeted delivery of development factors (read proteins and mRNAs) to the oocyte from the nurse cells [36,37]. At stage 10, given the scale of the oocyte and the large viscosity of its cytoplasm (about 1000 times that of water), it takes about a day to diffuse a large protein across the cell, whereas the flows reduce that to $\sim$30 min. Another answer might involve the mixing or suspending of nutrients needed for later development.

G. Modeling active microtubule beds: From discrete to continuum and back

A question dearer to our modeling hearts might be asking what mechanisms underlie the production of these flows. How are these flows created and how are they sustained? On this, the importance of the cytoskeleton, particularly microtubules and their associated kinesin-1 molecular motors, has long been recognized [38]. It has also become known that there is a population of long-lived microtubules situated near the cell wall [38]. Monteith *et al.* [39] proposed a fluid-structure model wherein kinesin-1 motors carry payloads away from the cell wall along flexible microtubules themselves clamped to a boundary. Newton's third law then dictates that the motor exerts a compressive force on the microtubule that is equal and opposite to the force the payload's upward motion exerts on the fluid. They simulated $\sim$100 motor-loaded, flexible microtubules above a no-slip plane and showed the emergence of an ordered flow reminiscent of streaming. While this simulation was provocative, one yearns for more insight into what controls the collective behavior and how the situation plays out in the setting of a closed cellular geometry.

To this end, with Cambridge colleagues, we first approached this problem by developing a coarse-grained model to capture and analyze collective behavior [41]. Hence, consider a large number N microtubules clamped to the inner surface of a spheroidal cell of effective radius W and surface area S ($\sim W^2$). As for the nuclear positioning problem discussed above, microtubules are modeled as inextensible elastic slender bodies (ϵ = microtubule radius/length $\sim 10^{-3} \ll 1$) [2,22] and the cytoplasm as a Newtonian fluid of viscosity μ [34]. The center-line shape of microtubule i at time t is $\mathbf{X}^i(s,t)$, where $0 \leqslant s \leqslant L$ is the arclength from its base and L its length (for simplicity, taken as identical for all microtubules). Microtubule shape evolution arises from balancing drag forces

with internal and imposed forces on the microtubule, and is here given by local slender-body theory [23,24,42],

$$\eta \mathbf{\Lambda}\left[\mathbf{X}_s^i\right]\left(\mathbf{X}_t^i - \bar{\mathbf{u}}^i(\mathbf{X}^i)\right) = \mathbf{f}^i - \sigma \mathbf{X}_s^i, \tag{1}$$

where $\mathbf{X}_s^i = \partial_s \mathbf{X}^i$ is the unit tangent vector to the microtubule center line, and $\mathbf{\Lambda}[\mathbf{X}_s^i] = \mathbf{I} - \frac{1}{2}\mathbf{X}_s^i \mathbf{X}_s^i$ is an anisotropic drag tensor with $\eta = 8\pi\mu/c(\epsilon)$ a drag coefficient ($c = |\ln e\epsilon^2|$ showing weak dependence on ϵ). The velocity $\bar{\mathbf{u}}^i$ is that induced by all other microtubules and backflow from the cortex. The force density $\mathbf{f}^i = -E\mathbf{X}_{ssss}^i + (T^i \mathbf{X}_s^i)_s$ is the elastic force due to microtubule bending, with rigidity E, and tensile forces, with tension T^i enforcing inextensibility. The microtubule aligned term $-\sigma \mathbf{X}_s^i$ is a coarse-grained compressive load ($\sigma > 0$) exerted by kinesin-cargo complexes.

Given the background fluid velocity, Eq. (1) describes an initial value problem for microtubule shape. The background cytoplasmic velocity $\mathbf{u}(\mathbf{x})$, induced by all microtubules and by periphery backflow, satisfies the forced Stokes equation,

$$-\nabla p + \mu \Delta \mathbf{u} = -\sum_{i=1}^{N} \int_0^L ds\, \mathbf{f}^i(s)\delta(\mathbf{x} - \mathbf{X}^i(s)); \; \nabla \cdot \mathbf{u} = 0, \tag{2}$$

where p is the pressure and no-slip is taken on the cortex. The minus ends of microtubules are pinned and clamped [respectively, $\mathbf{X}(0,t) = \mathbf{X}(0,0)$ and $\mathbf{X}_s(0,t) = \hat{\mathbf{n}}(\mathbf{X}(0,t))$ with $\hat{\mathbf{n}}$ the inward surface normal) at the cortex, and the free plus-end taken as torque and force free. That motor forces do not show up directly in determining the background velocity reflects their subdominant dipolar nature and the assumed close proximity of payloads to the load-bearing microtubules.

In addition to the motor force (per unit length) σ, there is the microtubule areal density $\rho = N/S$. From these devolve two essential control parameters, each a ratio of two timescales:

$$\bar{\sigma} = \frac{L^3}{E}\sigma = \frac{\tau_r}{\tau_m} \text{ and } \bar{\rho} = \frac{8\pi L^2}{c(\epsilon)}\rho = \frac{\tau_r}{\tau_c}. \tag{3}$$

Two of the timescales are $\tau_r = \eta L^4/E$, the single microtubule relaxation time arising from Eq. (1), and $\tau_c = \tau_r/\bar{\rho}$, a collective microtubule relaxation time arising from the forced Stokes Eq. (2). The remaining timescale is $\tau_m = \frac{L\eta}{\sigma}$, the motor transit time. Note that the collective relaxation time τ_c is potentially much faster than the single microtubule relaxation time τ_r [43].

In Ref. [41], we coarse-grained this model by assuming that microtubules were highly aligned and sufficient in number that their effect on the flow could be approximated by a continuum field. This builds on our previous modeling work (see Stein and Shelley [43]) and leads directly to an active porous medium model described by a Brinkman-Elastica equation. This system essentially evolves the Lagrangian flow map of the microtubule bed. We label the flow domain as Ω with boundary Γ, and subset $\bar{\Omega}(t) \subseteq \Omega$ which is the microtubule bed abutting Γ. The positional field $\mathbf{X}(\boldsymbol{\alpha}, s, t)$ of microtubule has the Lagrangian coordinates $\boldsymbol{\alpha} \in \Gamma$, where microtubules are pinned and clamped, and s, the microtubule arclength measured from the base; See the leftmost panel in Fig. 3(b) for a schematic. In dimensionless form, where we have used the microtubule length L as a characteristic length and τ_r as a characteristic time, the model reads:

$$\mathbf{\Lambda}[\mathbf{X}_s][\mathbf{X}_t - \mathbf{u}(\mathbf{X}, t)] = \mathbf{f} - \bar{\sigma}\mathbf{X}_s \tag{4}$$

$$-\nabla p + \Delta \mathbf{u} = -\bar{\rho}\, \mathcal{I}[\bar{\Omega}]\, [\mathcal{J}^{-1}(\boldsymbol{\alpha}, s)\, \mathbf{f}(\boldsymbol{\alpha}, s)]_{\mathbf{x}=\mathbf{X}(\boldsymbol{\alpha},s)} \text{ and } \nabla \cdot \mathbf{u} = 0. \tag{5}$$

where $\mathbf{f} = -\mathbf{X}_{ssss} + (T\mathbf{X}_s)_s$, $\mathcal{I}[\bar{\Omega}]$ is the indicator function of $\bar{\Omega}$, and $\mathcal{J}$ is the Jacobian of the deformation tensor $\frac{\partial \mathbf{X}}{\partial(\boldsymbol{\alpha}, s)}$. The Jacobian arises in converting the Lagrangian force density into an Eulerian one.

There are a number of interesting observations on the structure of this model:

(1) While perhaps not obvious, Eqs. (4) and (5) can be rewritten as a Brinkman-type model. Consider the system in the steady state with $\mathbf{X}_t \equiv \mathbf{0}$ and eliminate the force density $\mathbf{f}$ between them. This yields

$$-\nabla p + \Delta \mathbf{u} = \bar{\rho}[\mathcal{J}^{-1}\mathbf{\Lambda}[\mathbf{X}_s](\mathbf{u}(\mathbf{X}) - 2\bar{\sigma}\mathbf{X}_s)]_{\mathbf{x}=\mathbf{X}(\boldsymbol{\alpha},s)} \text{ for } \mathbf{x} \in \bar{\Omega}. \tag{6}$$

Equation (6) is a Brinkman fluid model with adimensional screening length $\sim\bar{\rho}^{-1/2}$, and a Brinkman drag force which is anisotropic (through $\mathbf{\Lambda}$) and relative to an active skeleton velocity $2\bar{\sigma}\mathbf{X}_s$. Interestingly, in the formal limit of large $\bar{\rho}$, with rescaling of p to retain incompressibility, this collapses to the anisotropic Darcy's law,

$$\nabla p = [\mathcal{J}^{-1}\mathbf{\Lambda}[\mathbf{X}_s](\mathbf{u} - 2\bar{\sigma}\mathbf{X}_s)]_{\mathbf{x}=\mathbf{X}(\boldsymbol{\alpha},s)} \text{ for } \mathbf{x} \in \bar{\Omega}, \tag{7}$$

suggesting that for large $\bar{\rho}$ the background velocity $\mathbf{u}$ should scale with the adimensional motor force $\bar{\sigma}$.

(2) There is a natural and instructive energy identity for Eqs. (4) and (5). The total elastic energy is stored in deformations of the microtubule bed,

$$\mathcal{E}(t) = \bar{\rho}\int_\Gamma dA_{\boldsymbol{\alpha}} \int_0^1 ds \frac{1}{2}\kappa^2, \tag{8}$$

where $\kappa = |\mathbf{X}_{ss}|$ is microtubule curvature. Accounting for all of the boundary conditions, $\mathcal{E}$ satisfies

$$\begin{aligned}\dot{\mathcal{E}}(t) &= \bar{\rho}\,\bar{\sigma}\int_\Gamma dA_{\boldsymbol{\alpha}} \int_0^1 ds(\mathbf{X}_t - \mathbf{u})\cdot(-\mathbf{X}_s) \\ &\quad - \left[2\|\mathbf{E}_\mathbf{u}\|_\Omega^2 + \bar{\rho}\int_\Gamma dA_{\boldsymbol{\alpha}} \int_0^1 ds(\mathbf{X}_t - \mathbf{u})\cdot\mathbf{\Lambda}\cdot(\mathbf{X}_t - \mathbf{u})\right] \qquad (9)\\ &= \mathcal{P} - \mathcal{D}, \qquad (10)\end{aligned}$$

where $\|\cdot\|_\Omega$ is the Frobenius tensor integral norm and $\mathbf{E}_\mathbf{u} = \frac{1}{2}(\nabla\mathbf{u} + \nabla\mathbf{u}^T)$ is the symmetric rate-of-strain tensor. The first term on the right-handside, $\mathcal{P}$, is the input power from motor loading. The second term, $\mathcal{D}$, is strictly negative and combines viscous dissipation and drag losses. Any nontrivial steady state, when $\mathbf{X}_t \equiv \mathbf{0}$ and $\dot{\mathcal{E}} = 0$, requires than $\mathcal{P} > 0$, or that the background velocity $\mathbf{u}$ and the microtubule tangent vector are, on average, coaligned.

(3) A telling feature of Eqs. (4) and (5) is its steady state of straight microtubules with no background flow:

$$\mathbf{X}_0(\boldsymbol{\alpha}, s) = \boldsymbol{\alpha} + s\mathbf{n}, \quad T_0(\boldsymbol{\alpha}, s) = -\bar{\sigma}(1-s) < 0, \quad \text{and } \mathbf{u}_0(\mathbf{x}) \equiv \mathbf{0}. \tag{11}$$

While there is no background flow, there is a negative tension proportional to the motor-load $\bar{\sigma}$. Hence, the microtubule bed is under compression, which is a recipe for a bend or buckling instability given sufficient motor loading.

In Stein *et al.* [41], we considered a two-dimensional and circular cell lined with a motor-loaded microtubule bed, and studied its axisymmetric dynamics. Linearization around the steady-state shown above combined with fully nonlinear, albeit axisymmetric, simulations produced a phase diagram of behaviors in $(\bar{\sigma}, \bar{\rho})$; aee Fig. 4(a). Of particular interest here is the existence of a a stable streaming state at sufficiently large $\bar{\sigma}$ and $\bar{\rho}$ (region IV). Nonlinear simulations in this circular geometry showed the course of the bending instability and led to the emergence of persistent axisymmetric streaming flow due to the inclination of the microtubules, and hence of their motor-protein induced forces, along the boundary; see Fig. 4(b). As suggested by comment (1) above, the induced streaming flow speed saturates with increasing $\bar{\rho}$ and increased with increasing $\bar{\sigma}$. As suggested by comment (2), the figure shows that the streaming flow is aligned with the bent microtubule bed as required by being in a nontrivial steady state.

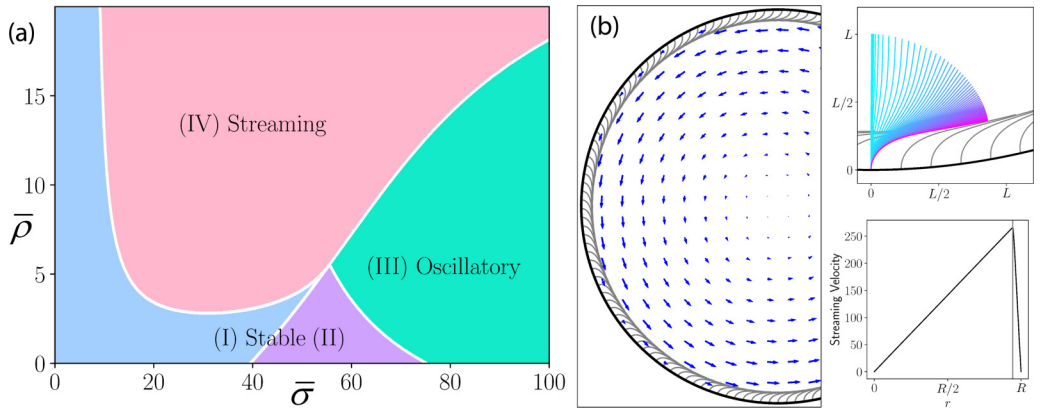

FIG. 4. (a) The phase diagram, over $(\bar{\sigma}, \bar{\rho})$, of growth rates and flow structure for model equations (4) and (5) when perturbed homogeneously from the straight microtubule case in a circular two-dimensional cell. In region I, growth rates are real and negative, while in region II the growth rates are complex with a negative real part and show damped oscillations. Region III has complex growth rates with a positive real part and show oscillatory dynamics. In region IV, the growth rates are real and positive and the microtubule bed bends collectively to produce streaming flows. (b) The fully developed steady-state streaming flow found through simulation. The upper right panel shows the microtubule bed evolution from being nearly straight to a bent canopy structure. Within the microtubule bed, the background flow is close to linear shear, with velocity rising and peaking at the edge of the microtubule canopy, with the inner flow being solid-body rotation. Adapted from Stein *et al.* [41].

This was strong theoretical evidence for a self-organizing cell-spanning flow arising from the motor-loaded microtubule bed. While very informative, its restricted nature—axisymmetry, two-dimensions, etc.—begged further examination of the system in more realistic settings.

H. Large-scale simulations of active beds in cellular geometries

Accordingly, in work with colleagues at Princeton and Northwestern, we turned to further experimental observations, and used SkellySim to simulate thousands of individual microtubules interacting over long times in closed cell geometries; see Dutta *et al.* [40]. Using the phase diagram as a guide and setting the discrete model first into spherical cells, in region IV of Fig. 4(a), we found the surprisingly robust emergence of cell-spanning, essentially axisymmetric streaming flows. To emphasize, this emergent axisymmetry now arises not by assumption but by the attraction of the system towards this state. Another important distinction with the two-dimensional model is that the three-dimensional spherical geometry disallows any homogeneous states (barring all microtubules being straight). This is essentially a manifestation of the hairy cueball, or Poincare-Hopf, theorem. Accordingly, the axisymmetric flow evinces two defects in microtubule orientation sitting at the two termini of the axis of the internal vortical flow; see Westwood and Keaveny [44] who discuss defects in the context of active fibers covering the *outside* of a mobile body. The defects discussed here are also associated with a secondary, inward axial flow whose combination with the dominating vortical flow we term a "twister." These simulations began with randomly distributed and straight (or nearly so) microtubules.

A comprehensive numerical study essentially recapitulated the phase diagram of behaviors in Stein *et al.* [41] with respect to $(\bar{\rho}, \bar{\sigma})$, though there was considerable interesting nonlinear dynamics revealed in the discrete microtubule simulations that were suppressed under the assumptions of the two-dimensional model. With respect to the emergence of twisters, this relaxation process was itself spatially complex but very robust to changes in microtubule locations or their initial shapes. Twister formation took place on the fast collective timescale τ_c, followed by long-time readjustments.

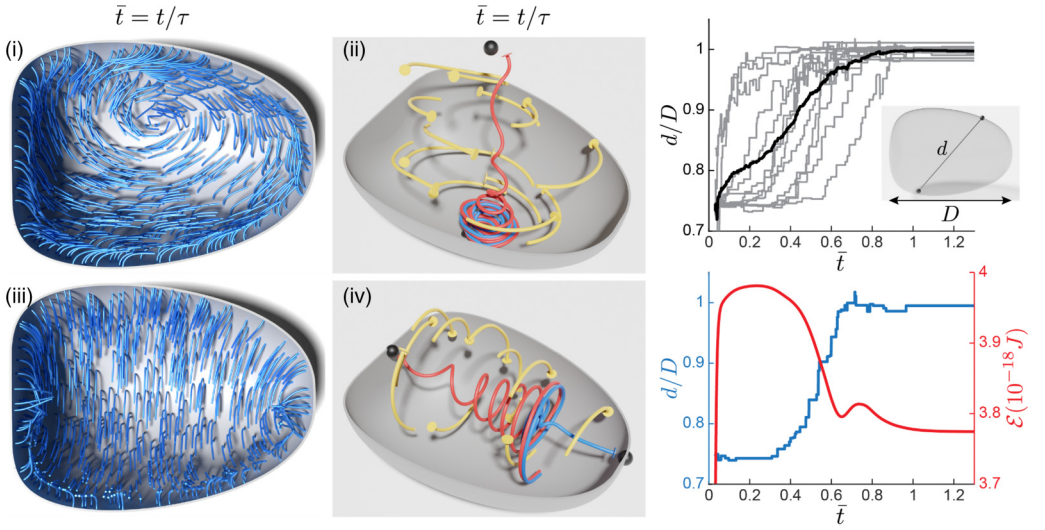

FIG. 5. (a) Dynamics of motor-loaded microtubules in an oocyte-shaped geometry. The top panel shows a cutaway view as the twister initially forms, with its vortex axis cutting across the short length of the cell. The twister's defect in microtubule orientation is clearly seen on the side of the cell, while its opposing defect is on the opposite face (not shown). (b) The flow streamlines at this time show the internal twister flow as a combination of a strong vortical component, plus a weaker inwards flow along the vortex axis. (c), (d) Over long times, the initially crosswise twister has rotated to align with the long axis of the cell, becoming nearly axisymmetric. Its streamlines retain the basic twister structure, though reoriented. The right uppermost panel shows the robust reorientation as initial data is varied. The right lower panel shows additionally, for the simulation in (i)–(d), the evolution of the elastic energy $\mathcal{E}(t)$ (red). Initally near zero, it rises rapidly on the τ_c timescale and peaks as the twister is formed. It then starts a slow decay, apparently on the τ_r timescale to a constant. Adapted from Dutta *et al.* [40].

Finally, given the symmetry of the cell shape, there was no geometrically preferred orientation or handedness for the emergent twisters.

However, as we remarked in our paper, oocytes are like cows; they are not spheres; at the stage when streaming first emerges, they instead resemble a nearly axisymmetric rounded cone. Simulations in such shapes show again the rapid formation of twisters at orientations that showed little respect to the cell symmetries. But, over long times, the internal twister axis rotates, with attendant defect motion, and moves into alignment with the axisymmetry axis of the cell; see Fig. 5.

This model can reproduce the flow speeds measured in real oocytes and provide an interpretation of the apparent variety of flow structures found in the stage-10 oocyte; see Dutta *et al.* [40]. While the initial twister formation takes place on the fast collective timescale τ_c, the slow relaxation to axisymmetry in simulation apparently takes place on the slow single microtubule relaxation time τ_r. If such a slow reorientation is taking place in experiments, it is likely happening on timescales beyond what we can observe in excised oocytes. On this latter question of axisymmetrization, we study the structure of oocytal flows in later stage egg cells, finding a predominance of apparently axisymmetric flows; see Jain *et al.* [45]. Finally, it is interesting to note the overall decrease in elastic energy $\mathcal{E}$ as the twister reorients in the cell. Interestingly, the lower energy axisymmetric twister puts beds of oppositely bent microtubules in closest proximity to each other, where their opposing flows can reduce bending and thus the elastic energy.

I. An active carpet model and a global attractor

Among many other unanswered questions is the robustness of the twister state. We have recently studied this question using a simplified active porous medium model [46], which we termed an

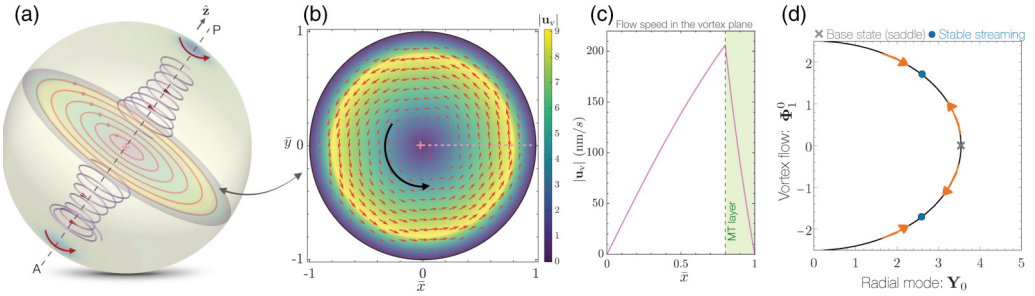

FIG. 6. Numerical and analytical results from the active carpet model. For a simulation with the initial **m** perturbed slightly from the inward normal **n**, (a)–(c) show the long-time flow as a twister. (a) Internal streamline structure as a dominant rotational flow plus a secondary, inwards axial flow. (b) Velocity field in the equatorial plane orthogonal to the vertical axis. (c) Rotational speed in this plane along a line from the vortical axis to the periphery. For a low order amplitude expansion, (d) shows the phase plot of the radial and vortical modes. The stable streaming state, marked as a blue dot, is the global attractor away from the purely radial and unstable base state. Adapted from Chakrabarti *et al.* [46].

active carpet. In this model, microtubules are replaced by a microtubule orientation, or polarity, field $\mathbf{m}(\boldsymbol{\alpha}, t)$ moving in a fluid sublayer of constant width H next to the cell boundary Γ. Bending rigidity, which seeks to straighten microtubules and bring them back to orthogonality with the cell surface, is replaced by a rotational spring at the microtubule base whose rest orientation is also orthogonal, and whose spring coefficient is tuned to give a relaxation time similar to that of a microtubule. In another interpretationthis simplified model describes straight microtubules attached to a rotationally compliant substrate. The effect of the microtubule bed in creating volumetric stresses is approximated by a stress jump, dependent upon microtubule density and motor strength, at the layer boundary with the bulk fluid inside the cell. Hence the model is a two-fluid system—with both the bulk and near -wall described by homogeneous Stokes equationsseparated by a dynamic stress jump that drives flows; details are found in Chakrabarti *et al.* [46]; see also Kimura *et al.* [11] for a related model.

Making the system nondimensional yields similar forms for $\bar{\rho}$ and $\bar{\sigma}$, while linear analysis and simulation in spherically shaped cells shows that this model behaves very similarly to the discrete many-microtubule model in the streaming flow region of $(\bar{\rho}, \bar{\sigma})$. Also, the system can be linearized about the steady-state $\mathbf{m} = \mathbf{n}$ and expressed in terms of spherical harmonics, with the associated fluid flows in the two-layer system diagonalized by a vector spherical harmonics basis for the Stokes equations. This gives an analytical expression for the growth rates of perturbations,

$$\lambda(l) = -1 + \left(\frac{R-1}{R}\right)^{l+2} \bar{\rho}(\bar{\sigma} - \beta), \tag{12}$$

where $R = W/H > 1$ and $\beta \sim |\ln \epsilon|^{-1}$ are geometric coefficients and $l \geqslant 1$ the polar index. Hence, the growth rates are independent of the azimuthal structure of the linear modes, and are maximal for $l = 1$. Of the three modes with $l = 1$, one is an axisymmetric mode resembling a cell-sized vortex. Having maximal growth rate at the largest system size, as here, is common to many active matter systems [47].

As described in Chakrabarti *et al.* [46] the nonlinear dynamics shows, as in Dutta *et al.* [40], a complex multimodal dynamics that relaxes robustly towards a twister state on the τ_c timescale. That emergent twister again combines a cell-scale vortical flow with a secondary bitoroidal component; see Figs. 6(a)–6(c). Because of the relative simplicity of the model, one can assume an expansion of **m** in a few low-order spherical harmonic modes, corresponding to a radially oriented mode that produces no flow, axisymmetric vortical and bitoroidal flows, and a nonaxisymmetric contribution. Insertion of this low-order expansion into the fully nonlinear dynamics is followed by Galerkin

projections of the dynamics, yielding a set of amplitude equations. These equations display a globally attracting steadystate that is a combination of the expansion's axisymmetric contributions, particularly the vortical and bitoroidal components. That is, it's a twister; see Fig. 6(d).

III. DISCUSSION

There remain, of course, many open problems and avenues of further work. I showed just a piece of our work on positioning, focusing on how advances in flow simulation, when combined with experiment, helped resolve a long-standing problem in intracellular force transduction. With the knowledge thus gained, we are attempting to build a biophysical model that captures, in an integrated way, how centrosomes guide the cell from fertilization to the first cell division. And of course, after the first cell division there will be others, all taking place within the original embryonic cell volume. This leads then to positioning problems in a plethora of cell shapes and sizes. How all of this happens robustly—again, again, and again—is an interesting problem.

Our work on oocytal flows is more conjectural and provocative. While our models capture important (or at least obvious) experimental observations, they are very stripped down. It is not actually clear what initiates these flows, what particular payloads are being carried by microtubule-associated motors, and many structural details of the microtubule beds are unknown. Answering such questions requires further engagement with experiment, and perhaps new or refined models. These flows are likely multifunctional and exactly what developmental purposes they serve—mixing or suspending of components, localization of important molecules, etc.—is ill-understood. There are other interesting transport and flow phenomena at play in oocyte development, such as along networks of microtubules threading through the egg chamber, localized flows between cells driven by dynein motors, and late stage dumping of contents by nurse cells into the oocyte. Finally, after fertilization the fruit fly embryo evinces a whole new set of fascinating fluid dynamics and positioning problems arising from the interaction of nuclei with the actomyosin layer at the cell wall. See Hernandez-Lopez *et al.* [48] for a recent study combining experiment, modeling, and flow simulation.

On a more general note, our quantitative understanding of biological processes will increasingly rest on interfacing experiments with modern tools of large-scale simulation, coarse-graining, and inference. The two problems I discussed both advanced through combining fluid dynamics simulation of discrete structures with the development and analysis of coarse-grain models. Inference against experimental data, gathered in concordance with modeling, will become an increasingly important quantitative task.

ACKNOWLEDGMENTS

I thank my many collaborators in these theoretical works, particularly B. Chakrabarti (ICTS Bangalore), Sa. Dutta (IIT-Bombay), R. Farhadifar (Flatiron), R. Goldstein (Cambridge), O. Jain (Princeton/Flatiron), D. Needleman (Harvard/Flatiron), S. Shvartsman (Princeton/Flatiron), and D. Stein (Flatiron). I especially thank B. Chakrabarti, R. Farhadifar, and David Stein for their comments on the paper and assistance with preparing figures.

[1] J. B. S. Haldane, On being the right size, Harper's Magazine 425 (1926).
[2] F. Gittes, B. Mickey, J. Nettleton, and J. Howard, Flexural rigidity of microtubules and actin filaments measured from thermal fluctuations in shape, J. Cell Biol. **120**, 923 (1993).
[3] K. Luby-Phelps, Cytoarchitecture and physical properties of cytoplasm: Volume, viscosity, diffusion, intracellular surface area, Int. Rev. Cytol. **192**, 189 (1999).
[4] D. Needleman and M. Shelley, The stormy fluid dynamics of the living cell, Phys. Today **72**(9), 32 (2019).

[5] B. Corti, *Osservazioni Microscopiche Sulla Tremella E Sulla Circolazione Del Fluido in Una Pianta Acquajuola* (Appresso Giuseppe Rocchi, Lucca, 1774).
[6] R. E. Goldstein and J.-W. van de Meent, A physical perspective on cytoplasmic streaming, Interface Focus. **5**, 20150030 (2015).
[7] R. Brown, *Observations on the Organs and Mode of Fecundation in Orchideae and Asclepiadeae* (Taylor, London, 1833).
[8] L. Pickens, *Organization of Cells and Other Organisms* (Clarendon Press, London, 1960).
[9] A. Mogilner and A. Manhart, Intracellular fluid mechanics: Coupling cytoplasmic flow with active cytoskeletal gel, Annu. Rev. Fluid Mech. **50**, 347 (2018).
[10] K. Yi, J. R. Unruh, M. Deng, B. D. Slaughter, B. Rubinstein, and R. Li, Dynamic maintenance of asymmetric meiotic spindle position through Arp2/3-complex-driven cytoplasmic streaming in mouse oocytes, Nat. Cell Biol. **13**, 1252 (2011).
[11] K. Kimura, A. Mamane, T. Sasaki, K. Sato, J. Takagi, R. Niwayama, L. Hufnagel, Y. Shimamoto, J.-F. Joanny, S. Uchida *et al.*, Endoplasmic-reticulum-mediated microtubule alignment governs cytoplasmic streaming, Nature Cell Biology **19**, 399 (2017).
[12] S. N. Hird and J. G. White, Cortical and cytoplasmic flow polarity in early embryonic cells of Caenorhabditis elegans, J. Cell Biol. **121**, 1343 (1993).
[13] M. Mayer, M. Depken, J. S. Bois, F. Jülicher, and S. W. Grill, Anisotropies in cortical tension reveal the physical basis of polarizing cortical flows, Nature (London) **467**, 617 (2010).
[14] A. G. Gubieda, J. R. Packer, I. Squires, J. Martin, and J. Rodriguez, Going with the flow: Insights from *Caenorhabditis elegans* zygote polarization, Phil. Trans. R. Soc. B **375**, 20190555 (2020).
[15] H.-Y. Wu, E. Nazockdast, M. J. Shelley, and D. J. Needleman, Forces positioning the mitotic spindle: Theories, and now experiments, BioEssays **39**, 1600212 (2017).
[16] H.-Y. Wu, G. Kabacaoğlu, E. Nazockdast, H.-C. Chang, M. J. Shelley, and D. J. Needleman, Laser ablation and fluid flows reveal the mechanism behind spindle and centrosome positioning, Nat. Phys. **20**, 157 (2024).
[17] S. Redemann, B. Weber, M. Möller, J.-M. Verbavatz, A. A. Hyman, D. Baum, S. Prohaska, and T. Müller-Reichert, The segmentation of microtubules in electron tomograms using amira, Mitosis: Methods Protoc. **1136**, 261 (2014).
[18] R. C. Wilson and J. A. Doudna, Molecular mechanisms of RNA interference, Annu. Rev. Biophys. **42**, 217 (2013).
[19] C. Garzon-Coral, H. A. Fantana, and J. Howard, A force-generating machinery maintains the spindle at the cell center during mitosis, Science **352**, 1124 (2016).
[20] K. Kimura and A. Kimura, Intracellular organelles mediate cytoplasmic pulling force for centrosome centration in the Caenorhabditis elegans early embryo, Proc. Natl. Acad. Sci. USA **108**, 137 (2011).
[21] T. Shinar, M. Mana, F. Piano, and M. J. Shelley, A model of cytoplasmically driven microtubule-based motion in the single-celled *Caenorhabditis elegans* embryo, Proc. Natl. Acad. Sci. USA **108**, 10508 (2011).
[22] M. J. Shelley, The dynamics of microtubule/motor-protein assemblies in biology and physics, Annu. Rev. Fluid Mech. **48**, 487 (2016).
[23] A.-K. Tornberg and M. J. Shelley, Simulating the dynamics and interactions of flexible fibers in stokes flows, J. Comput. Phys. **196**, 8 (2004).
[24] E. Nazockdast, A. Rahimian, D. Zorin, and M. Shelley, A fast platform for simulating semi-flexible fiber suspensions applied to cell mechanics, J. Comput. Phys. **329**, 173 (2017).
[25] O. du Roure, A. Lindner, E. N. Nazockdast, and M. J. Shelley, Dynamics of flexible fibers in viscous flows and fluids, Annu. Rev. Fluid Mech. **51**, 539 (2019).
[26] E. Nazockdast, A. Rahimian, D. Needleman, and M. Shelley, Cytoplasmic flows as signatures for the mechanics of mitotic positioning, Mol. Biol. Cell **28**, 3261 (2017).
[27] SkellySim cellular dynamics package, https://github.com/flatironinstitute/SkellySim (2022).
[28] D. B. Stein and M. J. Shelley, Computational tools for cellular scale biophysics, Curr. Opin. Cell Biol. **89**, 102379 (2024).

[29] Y.-N. Young, V. G. Herrera, H. Zhang, R. Farhadifar, and M. J. Shelley, A first-principles geometric model for dynamics of motor-driven centrosomal asters, bioRxiv (2024) [Phys. Rev. Res. (to be published)].
[30] M. E. Quinlan, Cytoplasmic streaming in the drosophila oocyte, Annu. Rev. Cell Dev. Biol. **32**, 173 (2016).
[31] J. Imran Alsous, N. Romeo, J. A. Jackson, F. M. Mason, J. Dunkel, and A. C. Martin, Dynamics of hydraulic and contractile wave-mediated fluid transport during *Drosophila* oogenesis, Proc. Natl. Acad. Sci. USA **118**, e2019749118 (2021).
[32] H. O. Gutzeit and R. Koppa, Time-lapse film analysis of cytoplasmic streaming during late oogenesis of *Drosophila*, Development **67**, 101 (1982).
[33] J. B. Glotzer, R. Saffrich, M. Glotzer, and A. Ephrussi, Cytoplasmic flows localize injected Oskar RNA in *Drosophila* oocytes, Curr. Biol. **7**, 326 (1997).
[34] S. Ganguly, L. S. Williams, I. M. Palacios, and R. E. Goldstein, Cytoplasmic streaming in *Drosophila* oocytes varies with kinesin activity and correlates with the microtubule cytoskeleton architecture, Proc. Natl. Acad. Sci. USA **109**, 15109 (2012).
[35] P. Khuc Trong, H. Doerflinger, J. Dunkel, D. St Johnston, and R. E. Goldstein, Cortical microtubule nucleation can organise the cytoskeleton of *Drosophila* oocytes to define the anteroposterior axis, Elife **4**, e06088 (2015).
[36] A. N. Becalska and E. R. Gavis, Lighting up mRNA localization in *Drosophila* oogenesis, Development **136**, 2493 (2009).
[37] W. Lu, M. Lakonishok, A. S. Serpinskaya, D. Kirchenbüechler, S.-C. Ling, and V. I. Gelfand, Ooplasmic flow cooperates with transport and anchorage in *Drosophila* oocyte posterior determination, J. Cell Biol. **217**, 3497 (2018).
[38] W. Lu, M. Winding, M. Lakonishok, J. Wildonger, and V. I. Gelfand, Microtubule–microtubule sliding by kinesin-1 is essential for normal cytoplasmic streaming in *Drosophila* oocytes, Proc. Natl. Acad. Sci. USA **113**, E4995 (2016).
[39] C. E. Monteith, M. E. Brunner, I. Djagaeva, A. M. Bielecki, J. M. Deutsch, and W. M. Saxton, A mechanism for cytoplasmic streaming: Kinesin-driven alignment of microtubules and fast fluid flows, Biophys. J. **110**, 2053 (2016).
[40] S. Dutta, R. Farhadifar, W. Lu, G. Kabacaoğlu, R. Blackwell, D. B. Stein, M. Lakonishok, V. I. Gelfand, S. Y. Shvartsman, and M. J. Shelley, Self-organized intracellular twisters, Nat. Phys. **20**, 666 (2024).
[41] D. B. Stein, G. De Canio, E. Lauga, M. J. Shelley, and R. E. Goldstein, Swirling instability of the microtubule cytoskeleton, Phys. Rev. Lett. **126**, 028103 (2021).
[42] J. B. Keller and S. I. Rubinow, Slender-body theory for slow viscous flow, J. Fluid Mech. **75**, 705 (1976).
[43] D. B. Stein and M. J. Shelley, Coarse graining the dynamics of immersed and driven fiber assemblies, Phys. Rev. Fluids **4**, 073302 (2019).
[44] T. A. Westwood and E. E. Keaveny, Coordinated motion of active filaments on spherical surfaces, Phys. Rev. Fluids **6**, L121101 (2021).
[45] O. Jain, B. Chakrabarti, R. Farhadifar, E. R. Gavis, M. J. Shelley, and S. Y. Shvartsman, Geometric effects in large scale intracellular flows, arXiv:2409.06763.
[46] B. Chakrabarti, M. Rachh, S. Y. Shvartsman, and M. J. Shelley, Cytoplasmic stirring by active carpets, Proc. Natl. Acad. Sci. USA **121**, e2405114121 (2024).
[47] D. Saintillan and M. J. Shelley, Active suspensions and their nonlinear models, C. R. Phys. **14**, 497 (2013).
[48] C. Hernández-López, A. Puliafito, Y. Xu, Z. Lu, S. Di Talia, and M. Vergassola, Two-fluid dynamics and micron-thin boundary layers shape cytoplasmic flows in early *Drosophila* embryos, Proc. Natl. Acad. Sci. USA **120**, e2302879120 (2023).